NUMERICAL MODELLING OF HYDRODYNAMIC BLADES AND FLOATING STABILITY OF MICRO HYDROPOWER STATION (PART 2)

NUMERICAL MODELLING OF HYDRODYNAMIC BLADES AND FLOATING STABILITY OF MICRO HYDROPOWER STATION (PART 2)

Viorel BOSTAN

Technical University of Moldova, bd. Stefan cel Mare 168, Chisinau,
viorel_bostan@mail.utm.md

***Abstract* – A new design and functional concept of a hydraulic flow turbine with vertical axis and individualized orientation of the hydrodynamic blades were proposed and elaborated. In order to maximize the flowing water energy conversion efficiency the hydrodynamic profile of the turbine blades is optimized taking into account the turbine dimensions, angle of attack and exploitation conditions. Since conversion efficiency highly depends on the hydrodynamic profile of the blades, it is important to minimize the deformations of the blades due to hydrostatic pressure and applied forces. Thus, there were performed deformation and stress analysis of the submersed hollow blade with metallic cover, blade injected with polyurethane foam with metallic cover and blade injected with polyurethane foam and composite material cover. Using the numerical results a suitable blade design, resistance structure and manufacturing technology are proposed. Also, the floating stability of 3- and 5-blades hydrodynamic rotor was analyzed. Based on carried out research, there have been elaborated two typo-dimensions of hydraulic turbines with 3 and 5 blades and optimal orientation of the blades with respect to the water stream direction. There were proposed, four different configurations of floatable micro hydropower stations for conversion of river kinetic energy into electric or mechanic energy.**

***Keywords*:** *hydraulic flow turbine, micro hydro power station, conversion of hydraulic energy.*

1. INTRODUCTION

Based on carried out research [1], there is proposed a constructive concept of two flow turbines with 3 and 5 blades with NACA hydrodynamic profile. These turbines have been used to design and manufacture four configurations of floatable micro hydro power stations for the conversion of river kinetic energy [2].
In order to increase the conversion efficiency it is necessary to optimize the hydrodynamic profile of the blades taking into account the turbine dimensions, angle of attack and exploitation conditions. Since conversion efficiency highly depends on the hydrodynamic profile of the blades, it is important to minimize the deformations of the blades due to hydrostatic pressure and applied forces. Therefore, it is important to design and analyze a resistance structure for the blades that will preserve the prescribed design shape parameters, along both the blade length and height.

2. OPTIMIZATION OF NACA 0016 HYDRODYNAMIC PROFILE

In order to maximize the torque produced by the micro hydro power plant rotor, the optimization of the hydrodynamic profile will be considered. The torque depends on the lift and drag hydrodynamic forces. The hydrodynamic forces through the hydrodynamic coefficients depend on the angle of attack α, Reynolds number Re and the shape of the hydrodynamic profile. The hydrodynamic shape of the profile was selected from the NACA 4 and 5 digit library of profiles having as parameter (considering the profile symmetry) only the maximal thickness. The angle of attack constitutes the second parameter. The optimization aims at maximizing the lift force and, at the same time, does not allow the pitching moment and the drag force to take very large values. The following optimization problem is considered:

$$\text{Maximize } C_L = C_L(\theta, \alpha)$$
$$\text{subject to constraints on } C_D \text{ and } C_M,$$

where θ is the maximum thickness and α is the angle of attack. The values of the lower and upper bounds are determined, as follows: the negative maximum value for the moment coefficient will correspond to the solution for the angle of attack 0^o. The maximum value for the drag coefficient will correspond to the solution for the angle of attack $\alpha = 18^\circ$. Also, restrictions have been added to the optimization parameters $10\% \le \theta \le 20\%$ and $0^o \le \alpha \le 20^o$. To find the optimal values of function $f = f(x_1, \ldots, x_n)$ an iterative method is used:

While given accuracy is not attained do,
Solve $B_i s_i = -\nabla f(x_i)$,
$x_{i+1} = x_i + \alpha_i s_i$,
End do

where α_i are the multipliers and B_i are the positive definite approximations of the Hessian of function f.

The partial derivatives of f are approximated with the finite difference formulas:

$$\frac{\partial f}{\partial x_i}(x) = \frac{f(x+he_i) - f(x-he_i)}{2h}, \qquad (1)$$

where e_i denotes the basis vector.

The optimization is implemented in MATLAB with a sequential quadratic programming algorithm with a line search and a BFGS Hessian update. The quadratic sub-tasks are solved by modified projection method. The gradient of function $C_L = C_L(\theta, \alpha)$ is approximated with finite differences with uniform step $h = 10^{-4}$. NACA 0016 profile was considered as initial profile. The result of the shape optimization procedure is presented in fig. 1.

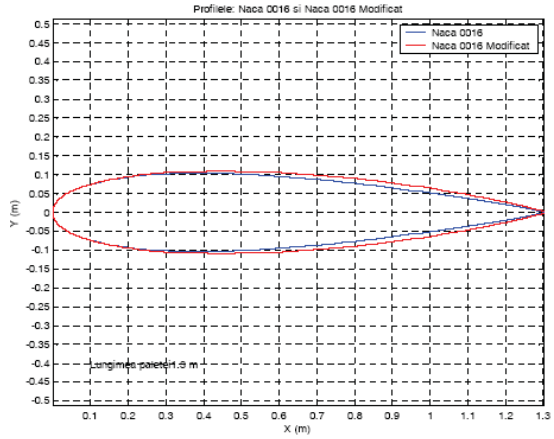

Figure 1: Standard and optimised NACA 0016 hydrodynamic profile.

3. COMPUTATIONAL SIMULATION OF WATER FLOW INTERACTION WITH HYDRODYNAMIC BLADES

In order to perform the deformation and stress analysis of a submersed blade with NACA 0016 hydrodynamic profile, the finite element ANSYS software is being used. Consider a submersed blade in the water flow subjected to hydrodynamic forces corresponding to the flow velocity $V_\infty = 2\,m/s$ and hydrostatic pressure [3]. The maximum value of the forces acting on the blade is 11 KN. The cover of the hydrodynamic blade is made of aluminium alloy H37 with Young module $E = 1.97 \cdot 10^{11}\ N/m^2$ and Poisson coefficient $\nu = 0.27$ and the blade's interior is hollow. Two values for the lateral cover thickness are considered: 1 mm and 1.5 mm. Also, three proposals for inner resistance structure of the blades have been examined: with 3, 4 and 5 transversal stiffening ribs. Fig. 2 shows the blade with 5 stiffening ribs. Since the estimated deformations can be considered small, the linear elasticity framework is adopted. The blade lateral cover is modelled with Kirchhoff-Love thin shell theory. The adaptive finite element discretization uses shell63 elements from ANSYS library [4]. The discretization with 18248 elements and 18683 nodes is shown in fig. 3. Forces applied on the discretized blade cover are presented in fig. 4.

The displacements in the blade lateral cover with thicknesses 1mm and 1.5mm and 5 transversal stiffening ribs are presented in fig. 5.

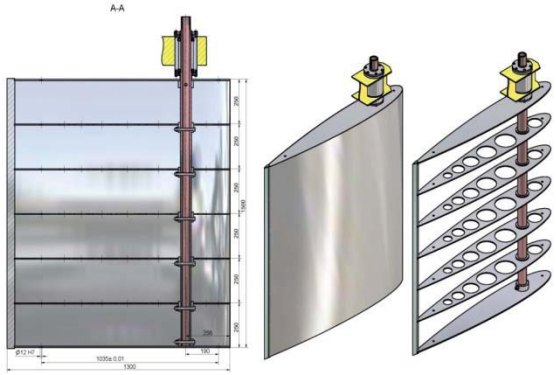

Figure 2: Resistance inner structure of the blade with 5 transversal stiffening ribs.

Figure 3: Discretization of the blade lateral cover into finite elements.

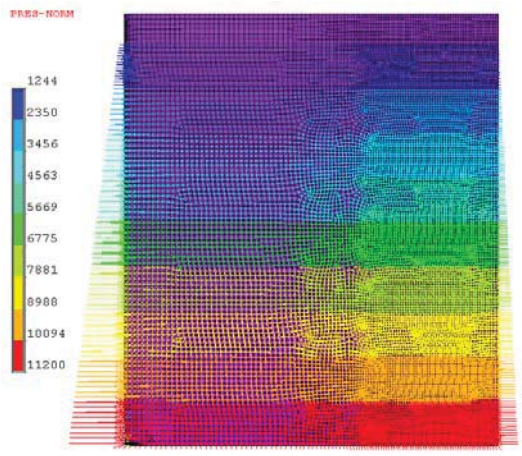

Figure 4: Forces applied on the discretized blade (N).

For the blades with lateral cover thickness of 1mm the maximal displacements in the lower submersed area are 7.8mm, 5.1mm and 3.5mm, respectively. These local displacements in the hydrodynamic profile can negatively influence the fluid flow regime in the adjacent zone and, consequently, the conversion efficiency of the water flow kinetic energy. For this reason, the profiles with the cover thickness of 1mm have been abandoned.

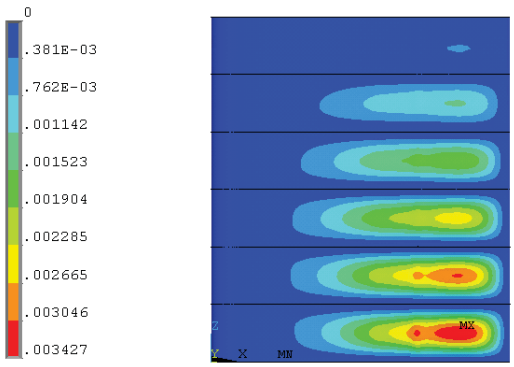

a.

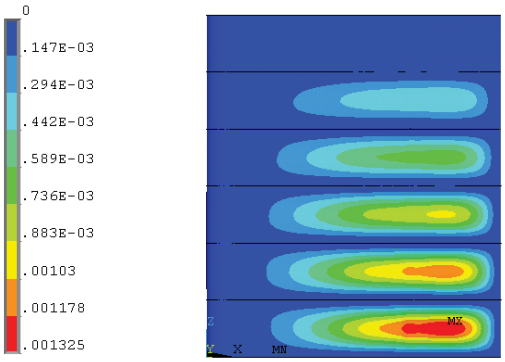

b.

Figure 5: Displacements (mm) in the NACA 0016 blade cover with 5 transversal stiffening ribs and thickness S=*1 mm* (a) and S=*1.5 mm* (b).

On the other hand, the maximal displacements in the blades with cover thickness 1.5mm and 3, 4 and 5 transversal ribs were reduced by 2.1, 2.4 and 2.6 times, respectively, totalling 3.7mm, 2.1mm and 1.3mm, respectively. The blades with the cover thickness 1.5mm and 5 transversal ribs have a maximal displacement of 1.33mm, acceptable from the point of view of decreasing the negative impact on the conversion efficiency. Therefore, the resistance structure with 5 transversal stiffening ribs and a lateral cover with thickness of 1.5 mm, made of aluminium alloy H37 will be examined further.

The conversion efficiency highly depends on the compliance with the prescribed design shape parameters, along both the blade length and height. Therefore, it is necessary to estimate the displacements along the blade length and height in the areas of maximal loading by hydrostatic and hydrodynamic forces. The displacements in the blade cover along the blade length in cross section located between the last two transversal ribs are shown in fig. 6(a). Thus, the maximum displacement of 1.3mm is located at a distance of 235mm from the trailing edge. The area with displacements larger than 1mm extends from a distance of 130mm to 530mm from trailing edge that consequently implies a local modification of the attack angle by ±0.29˚, a change hydro dynamically admissible. Fig. 6(b) shows the displacements from vertical cross section placed at a distance of 235mm from the blade trailing edge.

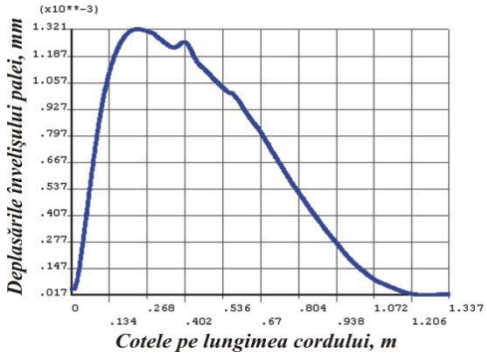

a.

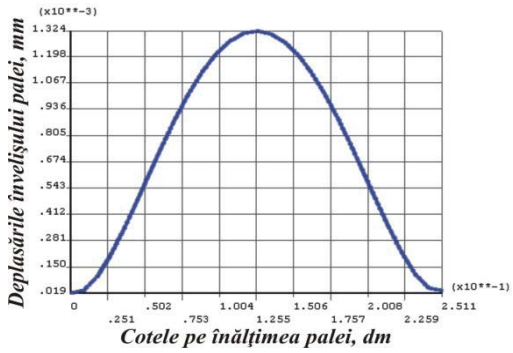

b.

Figure 6: Displacements (mm) in the blade cover in horizontal (a) and vertical (b) cross sections.

In order to quantify the stresses appearing in the blade cover with thickness 1.5mm consider the eigenvalues of stress tensor arranged in decreasing order, called the main stresses, σ_1, σ_2 and σ_3. Fig. 7 shows the distribution of σ_1(a) and σ_3(b). Also, consider the stress intensity and the Von Mises deformation, defined by:

$$\sigma_I = \frac{1}{\sqrt{2}}\left[(\sigma_1-\sigma_2)^2+(\sigma_2-\sigma_3)^2+(\sigma_1-\sigma_3)^2\right]^{1/2}, \quad (2)$$

$$\varepsilon_e = \frac{1}{\sqrt{2}(1+\nu)}\left((\varepsilon_1-\varepsilon_2)^2+(\varepsilon_2-\varepsilon_3)^2+(\varepsilon_1-\varepsilon_3)^2\right)^{1/2},$$

where ν is the Poisson coefficient, and $\varepsilon_1, \varepsilon_2$ and ε_3 are the eigenvalues of the deformation tensor. Fig. 8 shows the stress intensity and the Von Mises deformation in blade cover. From the analysis of the

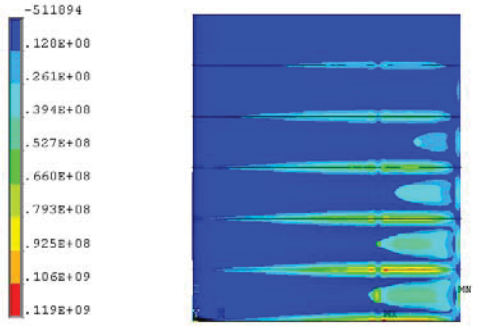

a.

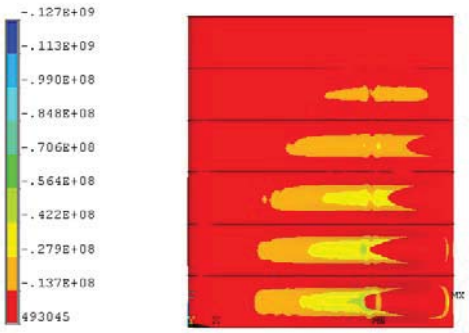

b.

Figure 7: Main stresses σ_1 (a) and σ_3 (b) (N/m2) in the blade cover with 5 transversal stiffening ribs.

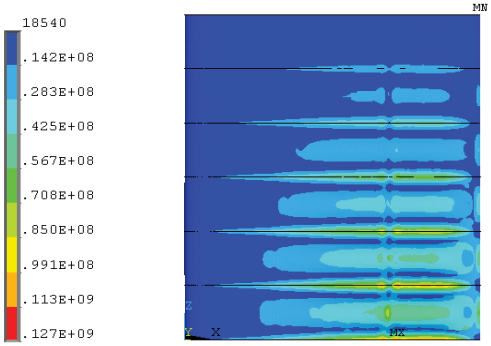

a.

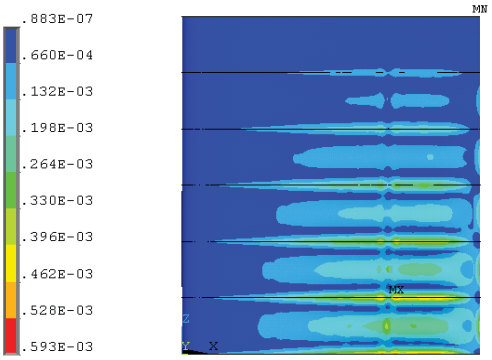

b.

Figure 8: Stress intensity (N/m^2) σ_I (a) and Von Mises deformation criterion ε_e (b) in the blade cover with 5 transversal stiffening ribs.

variation of stress intensity σ_I and Von Mises deformation in cross section along the blade length (fig. 9), the concentrations of stress intensity and Von Mises deformations were observed at a distance of 402mm from the trailing edge. This distance corresponds to the transition of NACA 0016 profile boundary from a region with lower curvature radius (distances 1137-402mm) to the region with a larger curvature radius (distances 402-0mm).

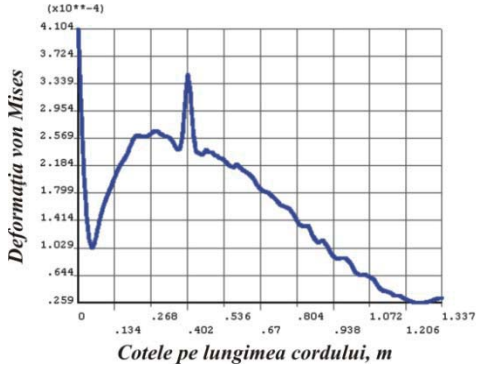

a.

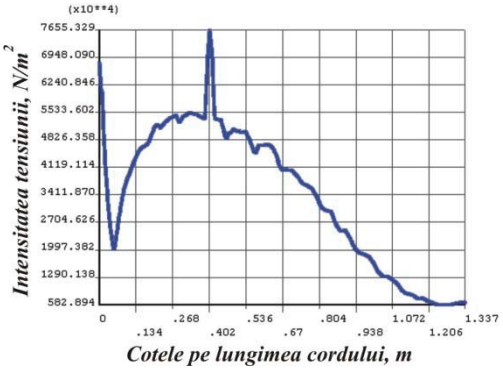

b.

Figure 9: Stress intensity (N/m^2) σ_I (a) and Von Mises deformation criterion ε_e (b) in cross section A of the blade cover.

Due to the fact that the blades of micro hydro power station will be acting in aggressive conditions (water and possible debris), an important issue consists in the assurance of the blades impermeability. For this purpose a hydrofoil injected with polyurethane foam should be also considered.

To this end consider a blade with cover made of aluminium alloy H37 with Young modulus $E = 1.97 \cdot 10^{11}\ N/m^2$ and Poisson coefficient $\nu = 0.27$ injected with polyurethane foam with density 0.6 kg/cm^3, Young modulus $E = 0.95GPa$ and Poisson coefficient $\nu = 0.24$. Since maximal deformations and stress occur between the last two stiffening ribs, only that portion of the blade was modelled. Discretization of the blade cover with 13340 elements Solsh190 is presented in fig. 10. The stiffening ribs are not modelled since their deformations are negligible, but

instead the constraints on the degrees of freedom are imposed: on line *A* (fig. 10) $u_x=0$, $u_y=0$ and $u_z=0$; on line B, $u_x=0$ and $u_y=0$; on line *C*, $u_z=0$. The polyurethane foam is modelled with 20785 elements of type Solid45.

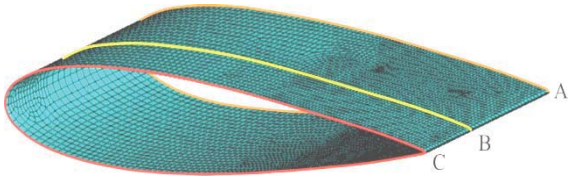

Figure 10: Discretization of the blade cover with Solsh190 finite elements.

The displacements in the blade injected with polyurethane foam and aluminium alloy cover with thickness 1.5mm are presented in fig. 11, u_x (a), u_y (b) and u_z (c), maximal displacement being 0.01 mm. In figure 12, there are shown the main stresses σ_1 (a), σ_2 (b) and σ_3 (c) (Pa). The maximal stress is of approximately 0.64 MPa.

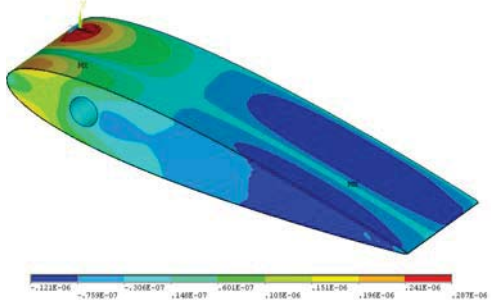

a.

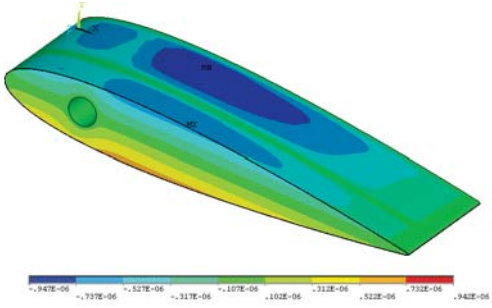

b.

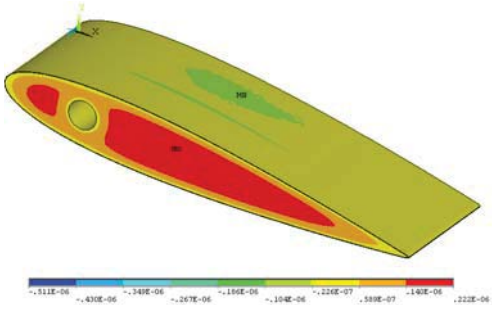

c.

Figure 11: Displacements in the blade injected with polyurethane foam and aluminium cover with thickness 1.5mm: u_x (a), u_y (b) and u_z (c).

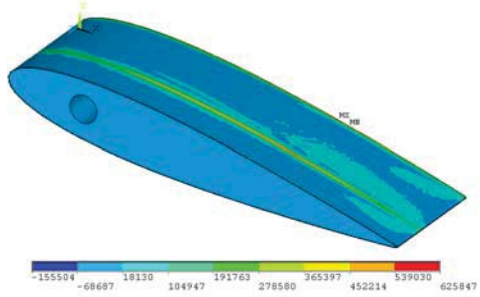

a.

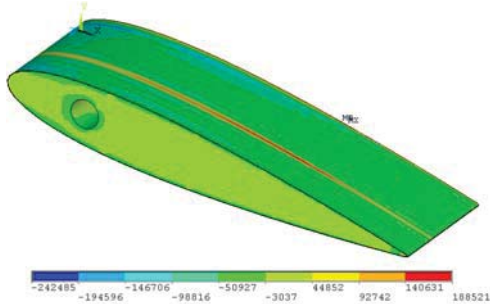

b.

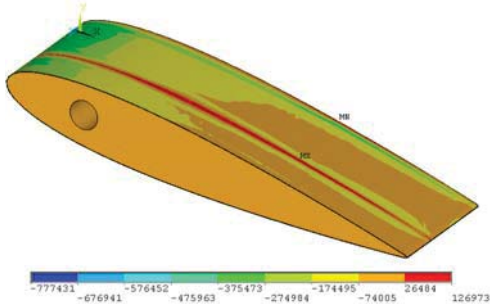

c.

Figure 12: Main stresses in the blade injected with polyurethane foam and aluminium cover with thickness 1.5mm: σ_1 (a), σ_2 (b) and σ_3 (c) (Pa).

On the other hand, since the manufacturing technology of the blades with aluminium cover needs expensive welding processes, special machines and qualified workers, it was proposed to use composite materials for lateral cover. Consider a laminated composite material shell composed of the following layers as shown in fig. 13: first layer bidirectional lining of type E fiberglass and polyetheric resin matrix; second layer has two sublayers consisted of chopped fiberglass linings with an armoured polypropylene lining between them; third layer is again a chopped fiberglass lining in a polyetheric matrix; and the fourth is a gelcout covering layer.

The computation of the material constants was performed using the manufacturer recommendations. The Young modulus for the composite layer is $E = E_m V_m + E_f V_f$, where E_m and E_f are Young modulus for matrix and fiberglass, respectively, and V_m and V_f are the volume fractions of the matrix and fiberglass. Evidently, $V_m+V_f=1$. Poisson coefficient is $\nu_{12} = \nu_m V_m + \nu_f V_f$, where ν_m and ν_f are matrix and

fibreglass Poisson coefficients. For the considered laminar plate (fig. 13) the volume fractions are V_m=0.5 and V_f=0.5. Thus, the following values have been obtained: Young modulus $E = 13.2GPa$ and Poisson coefficient $\nu_{12} = 0.3$.

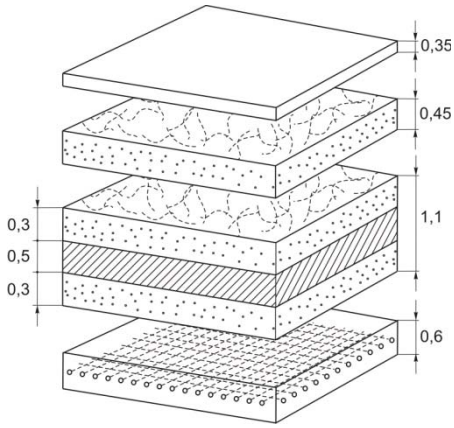

Figure 13: The structure of the composite material blade cover.

Two models have been considered: a portion of the hollow blade discretized with finite elements Solsh190 and a portion of the blade injected with polyurethane foam discretized with Solsh190 elements (lateral cover) and Solid45 elements (interior). In both cases the lateral cover is made of laminated composite materials with thickness 2.6mm, polyurethane foam material constants, hydrodynamic forces, hydrostatic pressure, constraints and boundary conditions. In the hollow hydrodynamic blade with composite material cover with thickness 2.6mm the maximal displacement is 4.3mm and the maximal stress value is approximately 38*MPa*. The stresses and displacement distributions are similar with those of hollow blade with aluminium cover. In fig. 14 there are presented displacements in the injected with polyurethane foam blade with the same thickness of lateral cover: u_x (a), u_y (b) and u_z (c), with maximal displacement 0.01mm. Fig. 15 shows the main stresses in a blade injected with polyurethane foam: σ_1 (a), σ_2 (b) and σ_3 (c) (Pa).

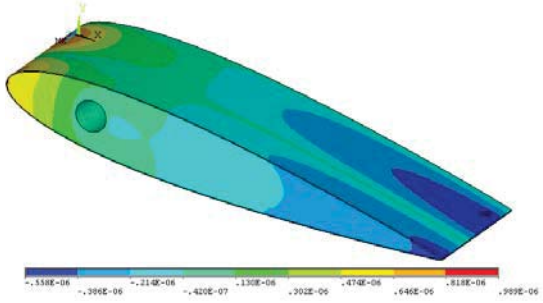

a.

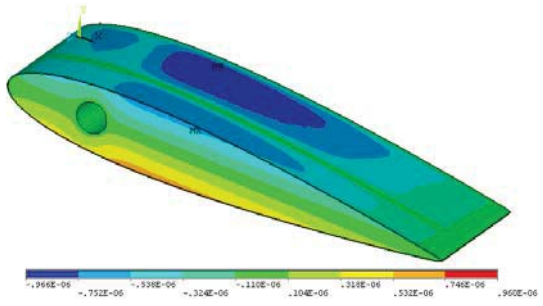

b.

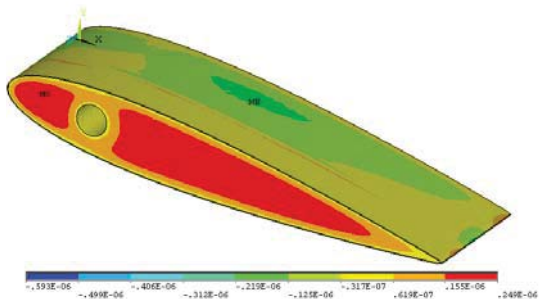

c.

Figure 14: Displacements in the blade injected with polyurethane foam and composite material cover with thickness 2.6mm: u_x (a), u_y (b) and u_z (c).

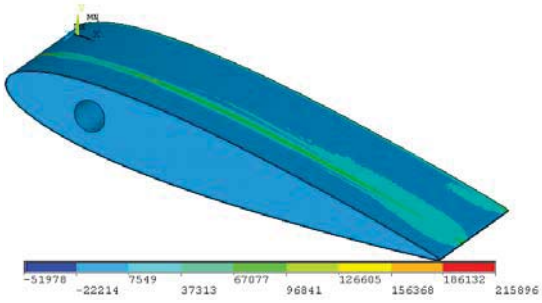

a.

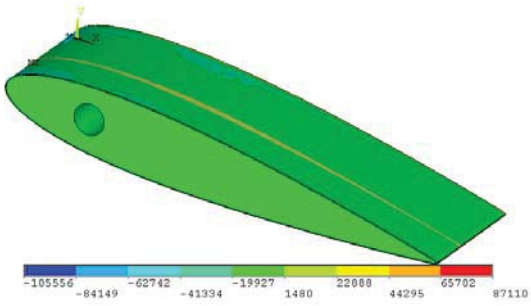

b.

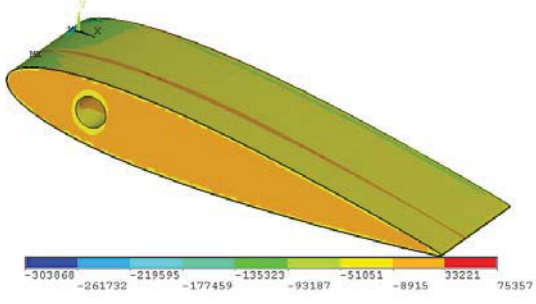

c.

Figure 15: Main stresses in the blade injected with polyurethane foam and composite material cover with thickness 2.6mm: σ_1 (a), σ_2 (b) and σ_3 (c) (Pa).

4. MANUFACTURING OF HYDRODYNAMIC PROFILE BLADES MADE OF COMPOSITE MATERIAL.

In order to increase the energy conversion and to reduce the production cost, modern technology for blade manufacturing from composite materials reinforced with fiberglass was developed. The developed technology comprises the following basic steps:

- design and manufacturing of the hydrodynamic profile moulding for the blade cover;

- elaboration of blade resistance structure;

- step-by-step layer shaping of the composite material;

- moulding of composite material coating, of resistance structure and injection with polyurethane foam.

The construction of the blade resistance structure (see fig. 2) complies with the manufacturing technology of the hydrodynamic blade cover with its partition along the symmetry axis (see fig. 16(a)). This allows the use of a single mould for the manufacturing of both parts of the blade cover. This constructive configuration of the blades ensures material savings and demands reduced labour force ensuring the manufacturing quality of the blade and complying with the geometrical parameters obtained from the theoretical calculation.

a.

b.

Figure 16: Mould for the manufacturing of the hydrodynamic blade cover from composite materials.

In fig. 17 there are presented the rotors of the hydraulic turbines with 3 and 5 hydrodynamic blades manufactured at Centre for Renewable Energy Conversion Systems Design of the Technical University of Moldova.

a.

b.

Figure 17: Manufactured rotors of the hydraulic turbines with 3 (a) and 5 (b) hydrodynamic blades.

5. FLOATING STABILITY OF THE MICRO HYDRO POWER STATION

Consider the micro hydro power station placed in the river water flow. The position of the blades with respect to the water level is ensured by the Archimedes forces acting on the floating blades. The blade cavity generates the Archimedes force given

$$F_A = \rho V g, \tag{3}$$

where ρ is the water density, V is the blade volume and g is the gravitational acceleration. The analysis of the trajectory of the application points of the Archimedes force F_A (points N_i, $i = 1,2,3$, fig. 18) has shown that the distance from these points to the rotor axis O will oscillate depending on the positioning angle φ. Thus, for the blades located in the upper half-plane defined by line OO' these distances are different from the respective distances of the blades located in the lower half-plane.

This fact leads to the appearance of the pitching moment with respect to the axis of longitudinal symmetry of the floating bodies:

$$M_r = M_{\Sigma,S} - M_{\Sigma,I}, \tag{4}$$

where $M_{\Sigma,S}$ is the total moment developed by the Archimedes forces that act on the blades, currently located in the upper half-plane, and $M_{\Sigma,I}$ is the total moment developed by the Archimedes forces that act on the blades currently located in the lower half-plane.

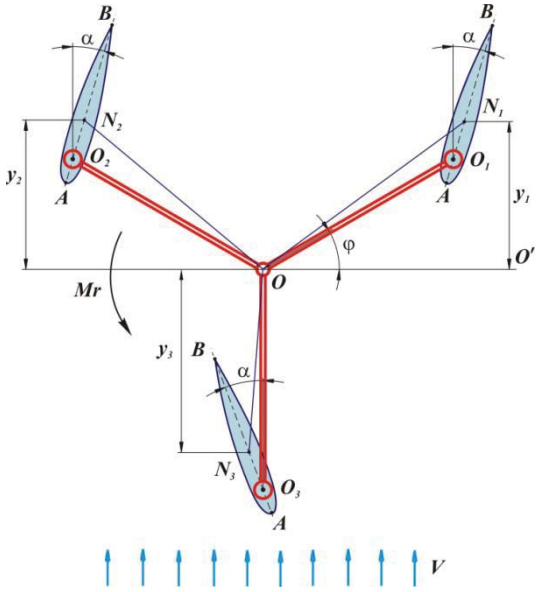

Figure 18: Floating stability analysis.

The total moments developed by the Archimedes forces that act on the blades currently located in the upper half-plane are determined by the relation

$$M_{\Sigma,S} = \sum F_{A,i} \cdot D_{A,i}, \tag{5}$$

where $F_{A,i}$ is the Archimedes force that acts on the blade i, $D_{A,i}$ is the distance from the application point of the Archimedes forces to the rotor axis, and the summation is done for all blades located in the upper half-plane. Similarly,

$$M_{\Sigma,I} = \sum F_{A,i} \cdot D_{A,i}. \tag{6}$$

Distances $D_{A,i}$ are given by:

$$D_{A,i}^2 = R^2 + c_A^2 + 2Rc_A \cos(\alpha + \varphi_i), \tag{7}$$

where R is the rotor radius, c_A is the distance between the application point of the Archimedes forces and the fixing point of the blade to the rotor lever, α is the angle of attack between the blade chord AB and the direction of water flow, and φ_i is the angle between the rotor lever and direction OO'.

In order to compensate for the resulting pitching moment M_r it is proposed to move the rotor axis position with distance e with respect to the plane of longitudinal symmetry of the floating bodies. Distance e is given by:

$$e = \frac{\sum_{i=1}^{N_{pal}} y_i}{N_{pal}}, \tag{8}$$

where N_{pal} is the number of rotor blades and y_i is the distance from the application point of the Archimedes force acting on blade i till the plane of longitudinal symmetry (fig. 18). For each blade, distance y_i is computed by:

$$y_i = c_A \cos\alpha + R\sin(\varphi + (i-1)\frac{360^o}{n}). \tag{9}$$

Substitute relation (5) into (4) to get:

$$e = c_A \cos\alpha. \tag{10}$$

The application point of the Archimedes force on each blade is the centroid of hydrodynamic profile, in this case NACA 0016 profile. The centre of application points of the Archimedes forces that act on a number N_{pal} of submersed blades will migrate during rotor revolution.

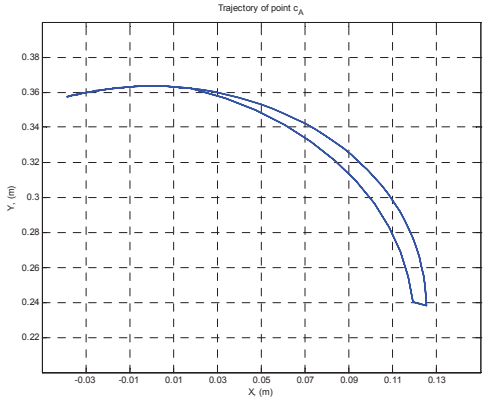

Figure 19: Migration trajectory of the central point of application of Archimedes forces for 3−blade rotor.

The migration trajectory generated by a full rotor revolution of 3−blade rotor represents the closed curve shown in fig. 19. A point on the closed curve corresponds to the position of the centre of application points of the Archimedes force system in a fixed angular position of the rotor.

To identify the technical solution ensuring the floating stability of the micro hydropower plant it is necessary to estimate the values of the distance between the centre of application point of the Archimedes force system and the longitudinal symmetry axis of the floating bodies. Fig. 20 shows the distance e versus the positioning angle φ of the 3-blade rotor. It has been established that in the case of a 3-blade rotor, distance e takes values bounded by $e_{min} = 0.238\ m$ and $e_{\max} = 0.363\ m$. For a 5-blade rotor, distance e is

bounded by $e_{min} = 0.289\ m$ and $e_{\max} = 0.363\ m$. The average value of distance e for both 3− and 5−blade rotors is $e_{ave} = 0.33\ m$.

In conclusion, in order to ensure the floating stability of the micro hydropower station the axis of 3- and 5-blade rotor must be shifted from the axis of longitudinal symmetry of the floating bodies at a distance of $e_{med} = 0.33\ m$ in the upriver direction. Also, micro hydropower stations anchored on the left bank must differ from those anchored on the right bank by the spatial truss constructions, in particular, by the constructional elements of the hydrodynamic rotor being shifted with distance eave.

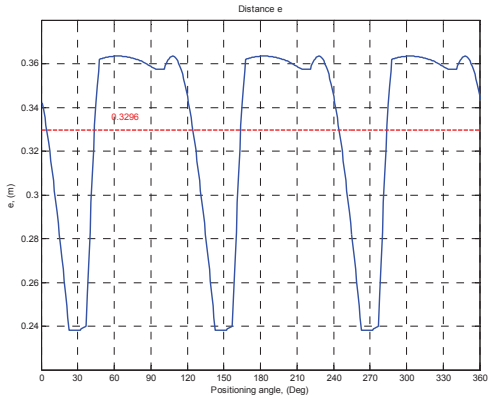

Figure 20: Distance e versus the positioning angle φ for the 3−blade rotor.

6. FLOATABLE MICRO HYDROPOWER STATIONS

Based on carried out research, there have been elaborated two typo-dimensions of hydraulic turbines with 3 and 5 blades and optimal orientation of the blades with respect to the water stream direction. There were proposed [2], four different configurations of floatable micro hydropower stations for conversion of river kinetic energy into electric or mechanic energy.

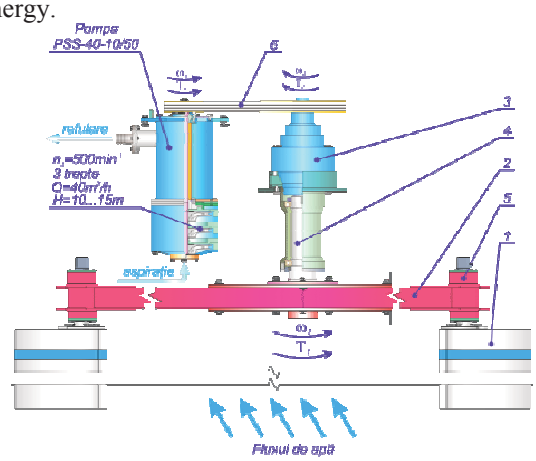

Figure 21: Kinematic scheme of a micro hydropower station: 1−blade, 2−rotor, 3−mechanical gear, 4,5−bearings, 6−belt drive.

Fig. 21 presents the kinematic scheme of the micro hydropower station MHCF D4x1,5M with 5 blades used for water pumping. In fig. 22, there is presented the constructive concept of micro hydropower station for electric energy generation MHCF D4x1,5E based on the hydraulic turbine with 5 blades. The blades 1 are mounted with bearings in rotor 2 coupled through a planetary gear 3 with electric generator 4. On the floating bodies 5 it is placed the spatial truss 7 coupled with the blades guiding and orientation mechanism 6.

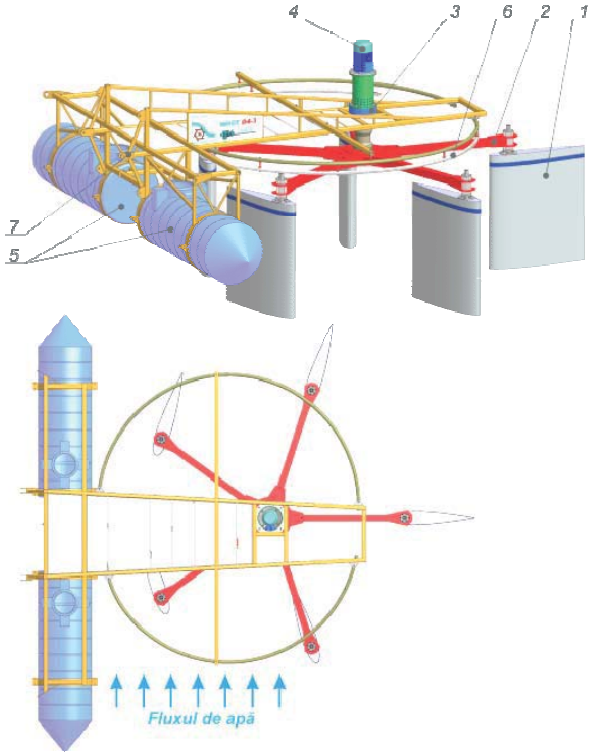

Figure 22: Micro hydropower station MHCF D4x1,5E.

Fig. 23 shows the micro hydropower station MHCF D4x1,5E for the conversion of river kinetic energy into electric energy manufactured at industrial enterprises from Republic Moldova, and fig. 24 presents the micro hydropower station installed on river Prut.

Figure 23: Micro hydropower station MHCF D4x1,5E.

Figure 24: Micro hydropower station MHCF D4x1,5E installed on river Prut.

The energy potential of the water flow and the power generated by the micro hydropower station are estimated for the following constructive and functional parameters (fig. 25): 5-blade rotor with diameter $D = 4m$, NACA 0016 modified hydrodynamic profile, immersed height of the blades $H = 1.4m$, length of the blade chord $c = 1.3m$, effective length of the blade chord $c' = 1m$, blade working angle of attack $\alpha = 18^o$.

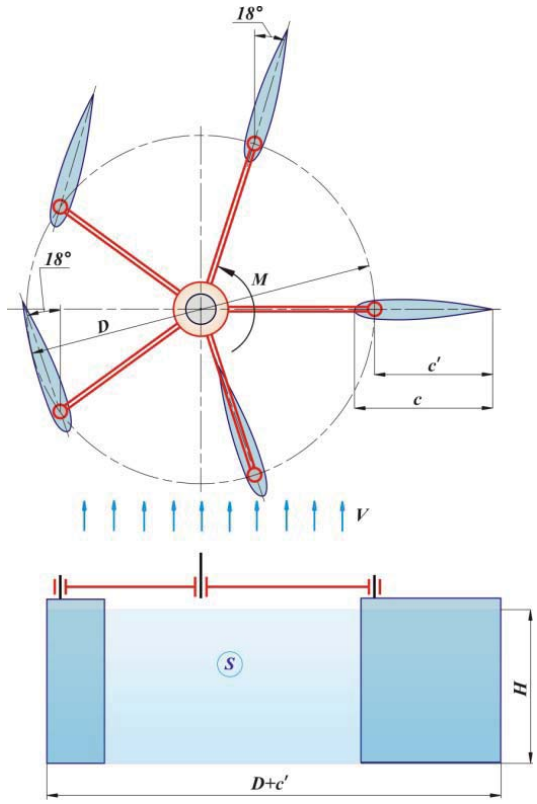

Figure 25: 5−blade hydrodynamic rotor.

Fig. 26 shows the converted power P_a at the rotor shaft versus the water flow velocity with a conversion efficiency coefficient 49.5% for various dimensions of the rotor cross section area $S = H(D + c')$: $7m^2$, $9.15m^2$ and $11.5m^2$.

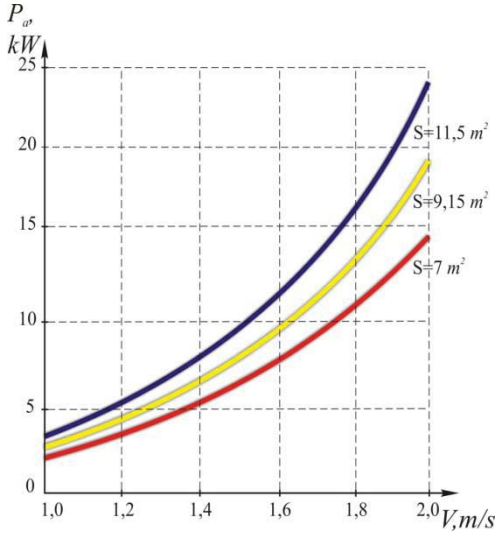

Figure 26: Generated power at rotor axis.

7. CONCLUSIONS

The blades with composite materials cover (thickness 2.6mm) injected with polyurethane foam and resistance structure with 5 stiffening ribs assure minimal local deformations that will not influence significantly the water flow and efficiency of energy conversion.

Experimental testing of the micro hydropower station MHCF D4x1,5E in real field conditions confirmed that the hydropower station with hydrodynamic 5−blade rotor assures the conversion of the energy at the rotor shaft to the generator clams with efficiency of 77.5%.

References

[1] V. Bostan, *Computational Analysis of Hydrodynamic Effects in Hydraulic Flow Turbines (Part 1),* 2011.

[2] I. Bostan, V. Dulgheru, V. Bostan, R. Ciuperca *Anthology of Inventions: Systems for Renewable Energy Conversion*, Technical University of Moldova, Chisinau, 2009.

[3] I. Bostan, V. Bostan, V. Dulgheru, *Numerical modelling and simulation of the fluid flow action on rotor blades of the micro-hydropower station*, Ovidius University Annals of Mechanical Engineering, Vol. VIII, Tom I, 2006, p.70-78.

[4] P. G. Ciarlet, *Mathematical Elasticity, vol.II. Theory of Plates,* Elsevier Science B.V., Amsterdam, 1997.

[5] R. M. Jones, *Mechanics of Composite Materials*, 2nd Edition, Taylor & Francis, 1999.

[6] MIL-HDBK-17 *Composite Materials Handbook*.

[7] ANSYS 10.0, *User's Guide*.

[8] ANSYS 10.0, *Advanced Analysis Techniques Guide.*